Neutron-scattering investigation of the electronic ground state of neptunium dioxide

1992 J. Phys.: Condens. Matter 4 3459

(http://iopscience.iop.org/0953-8984/4/13/010)

J. Phys.: Condens. Matter 4 (1992) 3459–3478. Printed in the UK

Neutron-scattering investigation of the electronic ground state of neptunium dioxide

G Amoretti†, A Blaise‡, R Caciuffo§, D Di Cola†, J M Fournier‡¶, M T Hutchings‖, G H Lander††, R Osborn‡‡, A Severing§§ and A D Taylor‡‡

† Dipartimento di Fisica, Università di Parma, Viale delle Scienze, I-43100 Parma, Italy
‡ Département de Recherche Fondamentale, Centre d'Etudes Nucléaires de Grenoble, 85 X, F-38041 Grenoble, France
§ Dipartimento di Scienze dei Materiali e della Terra, Università di Ancona, Via Brecce Bianche, I-60131 Ancona, Italy, and Istituto di Struttura della Materia del Consiglio Nazionale delle Ricerche, I-00044 Frascati, Italy
¶ Université Joseph Fourier, F-38000 St Martin D'Hères, France
‖ NDT Department, AEA In. Tec., Harwell Laboratory, Didcot, Oxon OX11 0RA, UK
†† Europäisches Institut für Transurane, Postfach 2340, D-7500 Karlsruhe 1, Federal Republic of Germany
‡‡ ISIS Facility, Rutherford Appleton Laboratory, Chilton, Didcot, Oxon OX11 0QX, UK
§§ Institut Laue–Langevin, Avenue des Martyrs, F-38042 Grenoble, France

Received 12 September 1991, in final form 19 December 1991

Abstract. Neutron spectroscopy has been applied to study the electronic ground state of NpO_2 both in the paramagnetic and in the ordered phase, below $T_c = 25$ K. The magnetic inelastic scattering cross section shows a broad peak which is split into two components and is centred at about 55 meV. This inelastic peak is shown to originate from excitations between the $\Gamma_8^{(2)}$ and $\Gamma_8^{(1)}$ crystal field quartets. Its position is in agreement with the value estimated by scaling the crystal field potential of UO_2 to the Np^{4+} case. Several mechanisms which could be responsible for the observed splitting are discussed. In the energy range below 15 meV the technique of polarization analysis has been used together with an incident polarized neutron beam to unambiguously separate magnetic from vibronic effects. At low temperature, below 25 K we see the appearance of an inelastic line (at an energy transfer of 6.4 meV) that indicates a lifting of the degeneracy of the Γ_8 ground state. This supports the hypothesis that the phase transition involves the quadrupolar ordering of the Np^{4+} ions by a collective Jahn–Teller distortion of the oxygen sublattice. The observed amplitude of the splitting is consistent with an oxygen displacement of the order of 0.02 Å, which is below the present limits of resolution of neutron diffraction experiments.

1. Introduction

Knowledge of the crystal field (CF) potential acting on the magnetic ions is often essential to describe the magnetic behaviour and thermodynamic properties of a compound. In actinides the CF is also important concerning the fundamental properties of the 5f electrons, such as their degree of localization and covalency or their participation in different interaction mechanisms. Because of the large radial extent of the 5f wavefunctions, the CF potential in actinides is strong, especially in oxides, and

0953-8984/92/133459+20$04.50

can produce overall splittings of the ground state manifold extending up to several hundreds of meV. For this reason, neutron spectroscopy studies of the CF in actinides have recently received a strong impulse with the advent of the new generation of spallation neutron sources which have an enhanced spectrum at epithermal energies.

Early investigations performed on UO_2 by Kern *et al* [1] at the Argonne National Laboratory showed the possibility of measuring CF excitations above 150 meV. The experiment on UO_2 was repeated at the spallation neutron source ISIS at the Rutherford Appleton Laboratory with improved energy resolution and extended the energy range to above 600 meV [2,3]. These measurements provided a complete determination of the CF potential and 5f-electron eigenstates for the U^{4+} ($5f^2$) ion in UO_2 and lead to new values of the cubic CF parameters: $V_4 = -123$ meV and $V_6 = 26.5$ meV. In the antiferromagnetic phase of UO_2 a splitting of the cubic CF levels due to the combined effects of the molecular field and triple-k distortion of the oxygen cage surrounding the U^{4+} ions was observed [3]. Experiments have also been performed to study the CF potential in both the paramagnetic and antiferromagnetic phases of the tetragonal compound UOS [4,5].

In this paper, we present the results of a neutron spectroscopy study of the CF excitations in NpO_2 involving three sets of experiments. This compound has the CaF_2 type crystal structure and is, therefore, isostructural to UO_2. Its lattice parameter at room temperature is $a_0 = 5.431$ Å. The Np ions have a tetravalent $5f^3$ electronic configuration [6], and ground state, in the Russell–Saunders (RS) coupling scheme, of $^4I_{9/2}$. The cubic CF potential leads to a $\Gamma_8^{(2)}$ quartet as ground state. At $T_c = 25$ K NpO_2 exhibits a phase transition, the origin of which is as yet unexplained despite considerable experimental and theoretical efforts devoted to its study. Although bulk property measurements such as specific heat [7] and susceptibility [8] indicate this phase transition by large anomalies, microscopic measurements such as Mössbauer spectroscopy [9] and neutron diffraction [10–12] have failed to find any evidence of magnetic ordering or lattice distortion. Similar anomalies observed in the isostructural compound UO_2 are due to a first-order phase transition from a paramagnetic to a type-I antiferromagnetic state [13,14] associated with a triple-k Jahn–Teller distortion of the oxygen sublattice [3]. The oxygen displacement is $\Delta_{3k} = 0.008$ Å, corresponding to $\Delta = 0.014$ Å if a monoclinic distortion is assumed [13,14]. Neutron diffraction experiments on NpO_2 are, however, more difficult because the available single crystals are quite small, the volume of the largest being of the order of 0.5 mm^3. As a consequence, only distortions larger than 0.02–0.03 Å could be resolved in the diffraction experiment so far performed.

The upper limit on the ordered magnetic moment set by Mössbauer spectroscopy is $\mu_0 < 0.01\ \mu_B$, to be compared with the effective Curie–Weiss paramagnetic moment of $\sim 3\ \mu_B$. If the magnetic moment is not ordered in the low-temperature phase, the magnetic susceptibility should diverge as the temperature decreases towards zero. However, the measured susceptibility reaches a constant value of 8.4×10^{-3} emu mol^{-1} at 5 K [8], which implies that the magnitude of the moment is almost zero. This is surprising since Np^{4+} is a Kramers ion ($5f^3$ electronic configuration) which cannot have a non-magnetic singlet as the CF ground state.

A direct determination of the CF parameters is therefore necessary to give an insight into the nature of the paramagnetic ground state and of the mechanism that may be responsible for the phase transition [15]. A previous attempt to observe the CF excitations in NpO_2 by neutron scattering [16] was not able to answer this problem

definitively; it did, however, show that sharp CF peaks were not present in NpO_2. In this respect NpO_2 and UO_2 are clearly different.

We have repeated the experiment under improved conditions at ISIS where, because of the greater flux available, we were able to use a sample having a mass ten times smaller. This considerably reduces the multiple phonon scattering as well as the self-heating problems inherent with the ^{237}Np α-activity.

Further experiments have been performed with lower incident energy at ISIS, and using polarization analysis at the Institut Laue–Langevin (ILL), Grenoble. The latter two experiments were aimed at studying the low-lying excitations. Two brief reports on some of the results obtained have been published elsewhere [17,18].

2. Experimental techniques

2.1. The neutron scattering cross section for unpolarized neutrons

Dipolar transitions between CF levels give rise to peaks in the neutron spectra, whose energies and intensities provide information on the eigenvalues and eigenfunctions of the CF Hamiltonian. The cross section for neutron-induced dipolar transitions between CF levels in localized electron systems is given by [19]

$$\frac{d^2\sigma}{d\Omega\, dE_f} = (\gamma_N r_0)^2[\tfrac{1}{2}g_J f(Q)]^2 \frac{K_f}{K_i} e^{-2W} \sum_{\alpha,\beta}(\delta_{\alpha,\beta} - \hat{Q}_\alpha \hat{Q}_\beta) \times \sum_{n\nu,m\mu} p_n \langle \Gamma_n^\nu | J_\alpha | \Gamma_m^\mu \rangle \langle \Gamma_m^\mu | J_\beta | \Gamma_n^\nu \rangle \delta(\hbar\omega + E_n - E_m) \quad (1)$$

where α, β are Cartesian coordinates, $J_{\alpha,\beta}$ is the total angular momentum operator, $|\Gamma_n^\nu\rangle$ are the CF eigenfunctions ν belonging to the energy level E_n with occupation probability p_n. Equation (1) holds for an array of non-interacting ions, unpolarized neutrons and small values of the momentum transfer $\hbar Q$. We use the conventional definition of scattering vector $Q = K_i - K_f$ and energy transfer $\hbar\omega = E_i - E_f$, where $E_{i(f)}$ and $K_{i(f)}$ are the incident (scattered) neutron energy and wavevector respectively. γ_N is the neutron magnetic dipole moment in nuclear Bohr magnetons, r_0 is the classical electron radius, g_J is the Landé factor, e^{-2W} is the Debye–Waller factor and $f(Q)$ is the 5f-electron form factor. The momentum transfer or Q-dependence of the cross section is dominated by the $f^2(Q)$ factor, which is a rapidly decreasing function of Q. In the case of Np^{4+} ions, the form factor is [20]

$$f(Q) = \langle j_0 \rangle + 1.75\langle j_2 \rangle \quad (2)$$

$\langle j_0 \rangle$ and $\langle j_2 \rangle$ being radial integrals calculated in the relativistic Dirac–Fock approximation by Desclaux and Freeman [21]. With Q in $Å^{-1}$, one has

$$f^2(Q) \sim \exp(-0.055Q^2). \quad (3)$$

This allows an easy distinction between magnetic and vibrational contributions, since the latter increases in intensity with Q. On the other hand, CF transitions may only be measured at small values of momentum transfer, and the kinematic constraint of the scattering process becomes particularly severe at high-energy transfer. Neutrons with high incident energy must then be used. For this reason, spallation neutron sources with a large flux in the epithermal region of the neutron spectrum are better suited than steady-state reactors to study magnetic excitations extending above 50–100 meV.

2.2. *Polarization analysis of neutron inelastic scattering*

This technique is described in the seminal paper of Moon *et al* [22]. The spin states of the scattered neutrons are analysed in the polarization direction z of the incident beam. Scattering events for which the neutron spin retains its initial orientation are referred to as non-spin–flip processes while the term spin–flip scattering is used to indicate events which reverse the direction of the neutron spin. Four spin-state cross sections may then be defined, with scattering amplitude given by

$$U^{ss'} = \langle s'|\hat{\sigma} \cdot \boldsymbol{D}_\perp|s\rangle \tag{4}$$

where $|s\rangle$ and $|s'\rangle$ may be either of the two neutron spin states corresponding to eigenvalues $+1$ and -1 for the z component of the Pauli spin operator $\hat{\sigma}$. The vector $\boldsymbol{D}_\perp$ is the projection of the Fourier transform of the magnetization operator $\boldsymbol{M}$ on a plane perpendicular to the scattering vector $\boldsymbol{Q}$:

$$\boldsymbol{D}(\boldsymbol{Q},t) = -\frac{1}{2\mu_B}\int \boldsymbol{M}(\boldsymbol{r},t)e^{i\boldsymbol{Q}\cdot\boldsymbol{r}}\,d\boldsymbol{r} \tag{5}$$

$$\boldsymbol{D}_\perp = \frac{1}{Q^2}(\boldsymbol{Q}\times\boldsymbol{D}\times\boldsymbol{Q}). \tag{6}$$

Equation (4) shows that fluctuations of $\boldsymbol{D}_\perp$ which are parallel to the quantization axis z give rise to non-spin–flip scattering, whereas fluctuations perpendicular to z produce spin–flip scattering. Therefore, if the neutron polarization $\boldsymbol{P}$ is along the scattering vector, the magnetic scattering is entirely spin–flip. On the other hand, the scattering length describing the interaction of the neutron with a nucleus of spin $\boldsymbol{I}$ is of the type

$$b = A + B\hat{\sigma} \cdot \boldsymbol{I} \tag{7}$$

where A and B are two constants whose values depend on the isotope. From equation (7) one may deduce that coherent and isotopic-incoherent nuclear scattering are non-spin–flip. Contributions of nuclear origin to the spin–flip cross section can only be caused by nuclear-spin incoherent scattering processes.

3. Experimental details

3.1. *Unpolarized neutrons*

The first experiment was performed using the direct-geometry chopper spectrometer HET of the ISIS facility [23]. Scattered neutrons are detected by two arrays of ^{3}He detectors, lying at 2.5 and 4 m from the sample position and covering a scattering angle range $\Delta\phi$ between 3° and 30°. A third detector array provides data at high angle $\phi = 136°$. Normalization of the spectra recorded at different angles is performed by measurements on a standard vanadium sample.

Incident energies of 25, 60, 120, 180, 600 and 1100 meV were used to study the scattering at different sample temperatures ranging from 5 to 50 K. The experiment was complicated by the presence of strong absorption resonances of Np at about 500 meV and above 1300 meV. This prevented us from using an incident energy

higher than $\sim$ 1200 meV, and caused a forbidden window in observable energy transfer between about 400 and 600 meV. Consequently, magnetic excitations could only be observed up to 350 meV at most. In fact, we have been unable to identify any purely magnetic scattering above $\sim$ 100 meV.

The sample used at ISIS spallation source consisted of 32 g of NpO_2 powder, with grains of about 50 μm in diameter, doubly encapsulated in a special Al holder. It was prepared at the Centre d'Etudes Nucléaires de Cadarache, France, by firing Np metal in oxygen atmosphere. Chemical analysis showed that impurities amounted in total to less than 250 ppm; x-ray diffraction patterns confirmed a single phase with lattice parameters corresponding to stoichiometric NpO_2. A sample of the isostructural compound ThO_2 (encapsulated in an identical container) was also measured in order to perform a detailed subtraction of the phonon contributions to the neutron spectra. ThO_2 has no 5f electrons and so only gives rise to nuclear scattering. On the other hand, its lattice constant (a = 5.56 Å) is very close to that of NpO_2, as are the nuclear scattering amplitudes of Th and Np. As a consequence, the neutron inelastic cross section for ThO_2 is expected to be very similar to the vibronic component in the NpO_2 spectra.

Measurements with smaller incident energies (E_i = 25 and 60 meV) at HET suggest that below 25 K an inelastic peak is present around $\sim$ 7 meV [18]. However, this is a difficult region in which to work because of the presence of strong single phonon lines, and we decided to use the method of neutron polarization analysis to identify the low-energy magnetic excitations.

3.2. Polarized neutrons

The experiment was performed on the IN20 three-axis spectrometer of the Institut Laue–Langevin, Grenoble, France, using a $\sim$ 10 g sample encapsulated in Al as a thin plate of $\sim$ 4 mm thickness. A horizontally magnetized Cu_2MnAl Heusler curved monochromator was used to polarize the incident beam and to select its energy. A similar Heusler analyser was employed to measure the energy and spin state of the scatterd neutrons. A flat-coil DC flipper installed between the monochromator and the sample position provided the possibility to reverse the polarization of the incident beam while a guide magnetic field was maintained along the flight path to preserve the spin state of the neutrons. A small magnetic field ($\sim$ 15 Oe), whose direction with respect to the momentum transfer Q is automatically controlled, was imposed at the sample position using a system of three Helmoltz coils. With the flipper ON, the spin–flip cross section $|U^{+-}|^2$ is measured, while the non-spin–flip cross section $|U^{++}|^2$ is obtained when the flipper is OFF.

All measurements were performed with the incident neutron polarization parallel to Q. In this case, the spin–flip and non-spin–flip scattering intensities, I_{SF} and I_{NSF}, are given by

$$I_{SF} = I_M + \tfrac{2}{3} I_{inc}^{s,n} + B_{SF} \tag{8}$$

$$I_{NSF} = I_{coh}^{n} + I_{inc}^{iso} + \tfrac{1}{3} I_{inc}^{s,n} + B_{NSF} \tag{9}$$

where I_M is the magnetic intensity, $I_{inc}^{s,n}$ and I_{inc}^{iso} are the nuclear-spin and isotopic-incoherent intensities, I_{coh}^{n} is the phonon scattering and B is the background. The incoherent scattering from the sample holder and cryostat is negligible; as it is also from the oxygen in NpO_2. For neptunium, the isotope-incoherent scattering is zero

but the nuclear-spin incoherent cross section is not known. However, if the energy of the system does not depend on the orientation of the nuclear spin, this latter contribution will be confined to the elastic line.

For safety reasons we were not allowed to change the incident wavevector during an experimental run, so that all measurements were performed in the constant K_i mode, using incident neutrons with energy $E_i = 34.8$ meV. The experimental data, after background subtraction, have therefore been corrected for a factor $(K_f^3 \cot \theta_A)$, to take into account the K_f/K_i dependence of the cross section and the variations of the reciprocal space volume accepted by the analyser as the energy of the scattered neutrons changes. Corrections have also been applied for the energy dependence of the analyser reflectivity, the absorption and the effects of incomplete polarization by the instrument (a flipping ratio $I_{OFF}/I_{ON} = 10.3$ was measured with no sample).

4. Data analysis and results

4.1. Unpolarized neutrons

The scattering functions $S(\phi,\omega)$ measured for NpO_2 and ThO_2 at an angle $\phi = 136°$ and $T = 5$ K, with an incident energy of 180 meV, are shown in figure 1. It is seen that the two spectra are nearly equal. At this angle Q varies between about 14 and 17 $Å^{-1}$ across the spectrum, and $f^2(Q)$ for the Np^{4+} ions is of the order of 10^{-7}. Figure 2 shows the neutron spectra obtained for NpO_2 and ThO_2 with $E_i = 180$ meV at an average angle of 5° ($1 < Q < 3$ $Å^{-1}$). No sharp excitation is observed, but extra intensity of presumably magnetic origin is clearly visible between ~ 30 and ~ 100 meV in the NpO_2 scattering function.

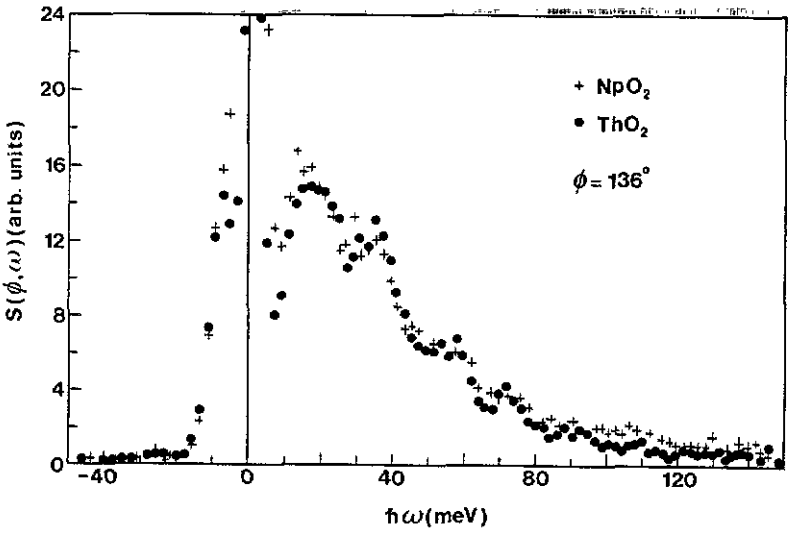

Figure 1. Inelastic neutron scattering cross section of NpO_2 (+) and ThO_2 (o) measured at $T = 5$ K with an incident energy of 180 meV. The scattering angle was $\phi = 136°$ and the scattering vector varies from about 17 to 14 $Å^{-1}$ as the energy transfer varies from 0 to 130 meV. Only vibronic contributions to the cross section are observed in these conditions.

In order to go beyond these qualitative observations, it is necessary to estimate the phonon scattering at low angles. This arises from both single scattering processes, whose cross section varies approximately as Q^2e^{-2W}, and multiple scattering processes. In slab geometry, with thin samples perpendicular to the incident beam, multiple scattering is approximately isotropic, except at scattering angles close to 90°. It therefore forms the dominant contribution to the low-angle spectra because of the Q^2 factor in the single phonon cross section. On the other hand, the 136° spectra are dominated by single scattering processes, except at energy transfers above the single-phonon density-of-states where only multiple scattering and the small multi-phonon cross section can contribute. Figure 3 shows the experimentally determined ratio of the 5° to 136° scattering from ThO_2 as a function of energy transfer. This ratio, $r(\hbar\omega)$, increases with $\hbar\omega$ because of the contribution from multiple inelastic processes, and reaches a plateau value of ~ 1.0 at high energies. Monte Carlo calculations of multiple scattering in vanadium predict a similar functional form for $r(\hbar\omega)$ [24].

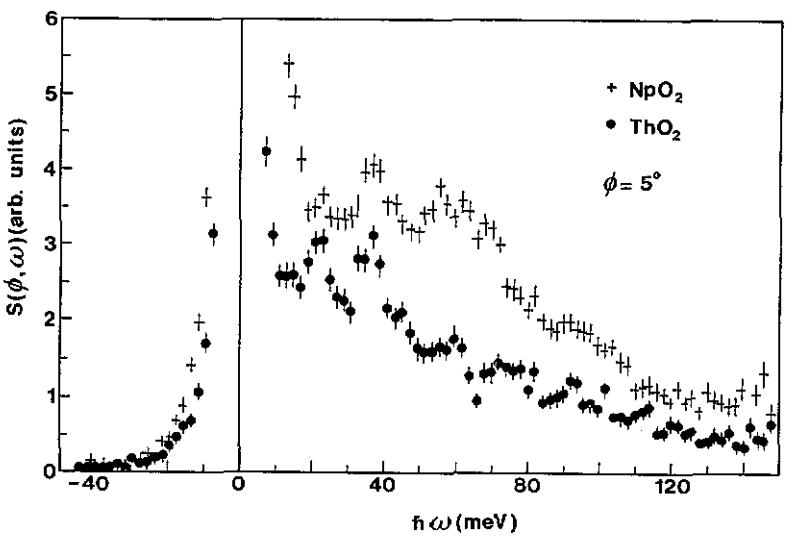

Figure 2. Neutron spectra measured with an incident energy of 180 meV at a scattering angle $\phi = 5°$ for NpO_2 (+) and ThO_2 (o) at a temperature of 5 K. Extra intensity of magnetic origin is visible in the NpO_2 cross section. The variation of the scattering vector with energy transfer is from about 3 to 1 $Å^{-1}$, as the energy transfer varies from 0 to 120 meV.

The assumption we make is that the scaling function, $r(\hbar\omega)$, derived from the experimental ThO_2 data, may also be used to estimate the 5° phonon scattering in NpO_2. This is reasonable given the similarity in the nuclear cross section of both materials (figure 1). To obtain the magnetic scattering, therefore, we have multiplied the NpO_2 136° spectrum by $r(\hbar\omega)$, shown as the full curve in figure 3, before subtracting it from the 5° spectrum. The results of this procedure are shown in figure 4, where we have terminated the plots at 25 meV. Below this value the scattering is contaminated by the incoherent elastic signal and the subtraction procedure is less reliable.

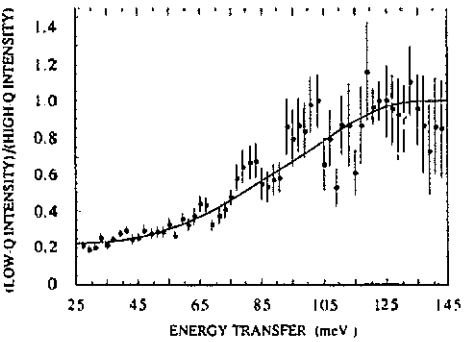

Figure 3. Energy dependence of the ratio $r(\hbar\omega)$ of the ThO_2 spectra measured at scattering angles $\phi = 5°$ and $\phi = 136°$. The full curve is the best fit to the data.

The results of the phonon subtraction outlined earlier are shown in figure 4 for four different temperatures, both above and below the phase transition at $T_c = 25$ K. A broad magnetic signal centred at about 55 meV, which appears to be split into two components, is positively identified. Scans using higher incident energy did not reveal any other peak up to at least 350 meV.

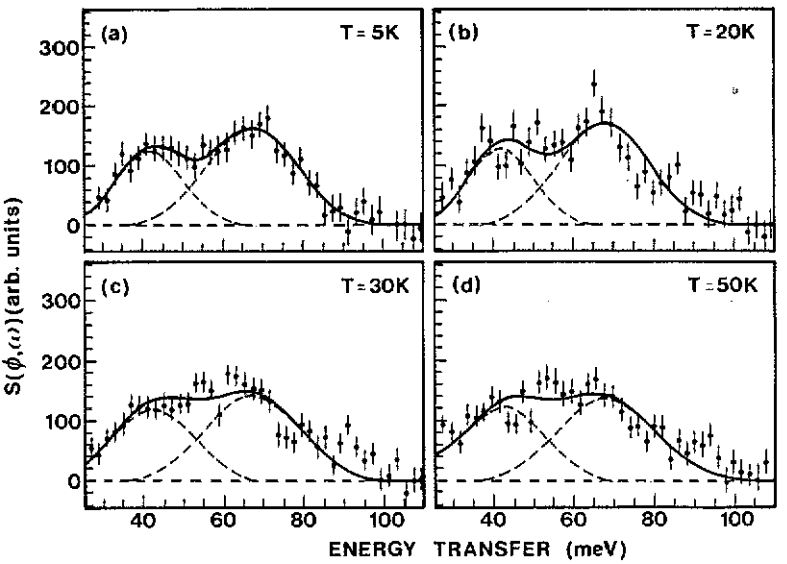

Figure 4. Inelastic magnetic neutron scattering cross section obtained for NpO_2 at $T =$ (*a*) 5, (*b*) 20, (*c*) 30 and (*d*) 50 K. The incident energy was 180 meV and the average scattering angle $\phi = 5°$. The phonon contribution has been removed following the procedure described in the text. The full curve is a fit to the data of Gaussian profiles and a sloping background. These components are shown by the broken curves.

The same procedure described previously for the subtraction of the phonon contribution has been applied in the analysis of the scattering function measured at four different angles, 11.5°, 16.5°, 21.5° and 26.5°, in order to follow the Q-dependence of the integrated intensity of the magnetic signal.

The profile of the inelastic signal changes only slightly with the temperature and

the angle, and can be fitted by two Gaussian functions. The first subpeak is centred at ~ 42 meV and the second more intense one at ~ 67 meV. The full width at half maximum (FWHM) of the first subpeak is about 21 meV, and that of the second one about 26 meV. These widths tend to increase with increasing temperature.

4.2. Polarized neutrons

Figure 5 shows the raw data obtained for the spin–flip intensity in the constant-Q mode ($Q = 1.9$ Å^{-1}) at two temperatures, $T = 5$ K and $T = 50$ K. Comparison with the non-spin–flip intensity, also shown in figure 5, reveals that magnetic scattering is present both above and below the phase transition. However, at low temperature the magnetic response consists of an inelastic peak centred at about 6.4 meV whereas, above the phase transition, the magnetic intensity distribution appears to be centred at zero energy transfer.

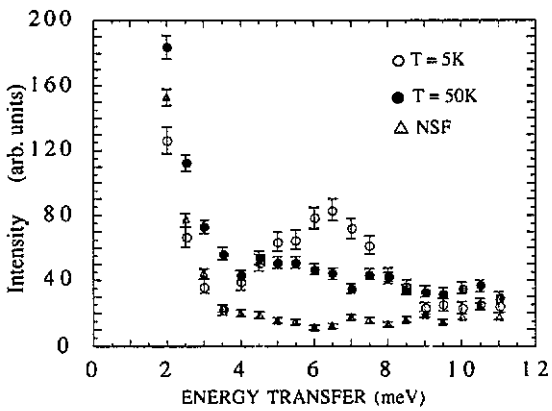

Figure 5. Spin–flip intensity obtained at $T = 5$ and $T = 50$ K for a Q value of 1.9 Å^{-1}. The non-spin–flip intensity (△), which appears to be temperature independent, is also shown for comparison.

The results obtained at different temperatures, after the corrections described in section 2.2, are shown in figure 6 to illustrate how the magnetic response changes through the phase transition. Below 25 K, the data may be fitted to a Gaussian lineshape with almost constant area but with a FWHM which increases from 3.4 meV at 5 K to 5.3 meV at 20 K. This figure must be compared with the instrument energy resolution which is about 3 meV. At the same time, the peak position shifts from 6.4(1) to 5.9(1) meV. The polarization analysis results also show that continuous magnetic scattering is indeed present above the phase transition. It may be fitted to a Lorentzian profile times energy centred at zero energy transfer multiplied by the Bose thermal factor. The integrated intensity, which is of the same order of magnitude as that observed in the low-temperature phase, does not change appreciably up to 50 K. On the other hand, a slight variation in the FWHM, from 9.8(9) to 11.7(8) meV, is observed as the temperature increases from 25 to 50 K.

In a second part of the experiment we searched for the appearance below the phase transition of magnetic Bragg scattering. A very weak and broad magnetic reflection was in fact observed [25, 26] around the $[\frac{1}{2}\frac{1}{2}\frac{1}{2}]$ lattice point for the $U_{1-x}Np_xO_2$ solid solution, with $x = 0.5$ and $x = 0.75$. The results reported in [25, 26] suggest that, in the Np-rich solid solution, short-range magnetic order with a configurational

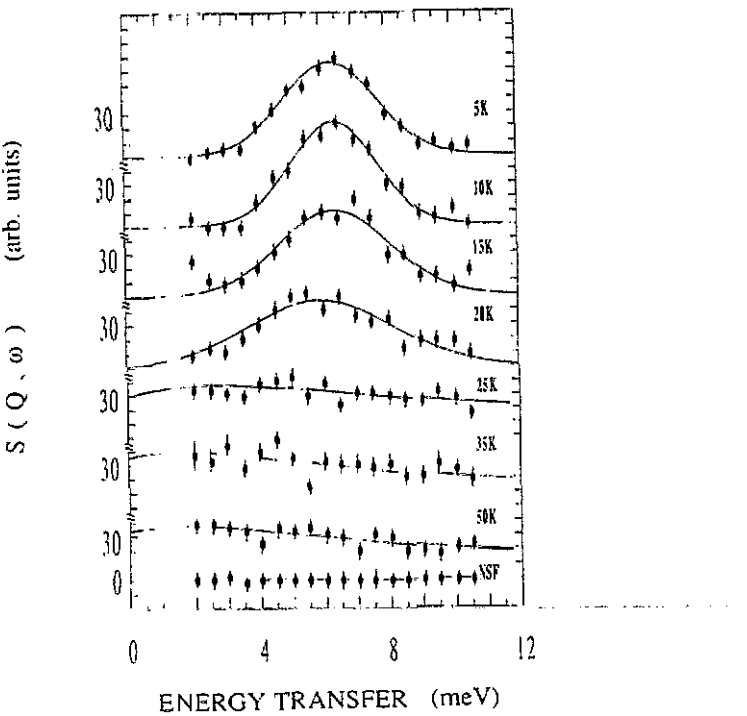

Figure 6. Evolution of the spin–flip scattering function as the temperature is increased through the phase transition point. $Q = 1.3$ Å^{-1}. The full curves are the best fit to the data with a Gaussian lineshape below 25 K or, above the phase transition, with a Lorentzian profile times energy centred at zero energy transfer and multiplied by the Bose thermal factor.

symmetry different from the one of UO_2 occurs, the correlation length being estimated as 30–60 Å. In the experiment currently being reported, data were therefore collected as in a powder scan with the analyser set for elastic scattering. For intensity reasons, unpolarized neutrons were used with pyrolytic graphite as monochromator and analyser. Two spectra were recorded, at 5 and 50 K, with incident energy $E_i = 35.1$ meV and Q varying between 0.8 and 1.8 Å^{-1}, i.e. from the $[\frac{1}{2}\frac{1}{2}\frac{1}{2}]$ to the [110] lattice positions. No magnetic Bragg scattering was found at low-temperature. From the standard deviation on the background and the intensity measured for the [111] nuclear Bragg peak we estimate an upper limit of $\sim 0.5\ \mu_B$ for any ordered component of the moment.

5. Interpretation of the data

5.1. The cubic phase

The $5f^3$ configuration of the free Np^{4+} ion consists of 41 multiplets, labelled $^{2S+1}L_J$ in the Russell–Saunders (RS) coupling scheme. Hund's rules give the $^4I_{9/2}$ as ground state. In the cubic crystalline environment of NpO_2, the tenfold degeneracy of this lowest manifold is lifted by the CF potential into a $|\Gamma_0\rangle$ doublet and two quartets, $|\Gamma_8^{(2)}\rangle$ and $|\Gamma_8^{(1)}\rangle$. The total Hamiltonian of the $5f^3$ configuration may be written as

the sum of two terms

$$H = H_{\text{ion}} + H_{\text{CF}} \tag{10}$$

with

$$H_{\text{ion}} = H_{\text{C}} + H_{\text{SO}} + H_{\text{int}}. \tag{11}$$

Here, H_{C} is the Coulomb repulsion between the three f electrons, parametrized by the Slater integrals $F^{(2)}$, $F^{(4)}$, $F^{(6)}$, and H_{SO} is the spin–orbit interaction, characterized by the coupling constant ζ_{SO}. H_{int} describes the configuration interaction (CI), that is the mixing of higher-lying electronic configurations into the $5f^n$ configuration, and other interactions arising from the couplings of the orbital and spin angular momenta of different electrons (orbit–orbit, spin–spin, spin–other-orbit). CI acts as a screening mechanism weakening the 5f Coulomb potential due to the fact that $5f^n$ electrons spend part of their time in more delocalized states. The overall effect of H_{int} is, however, much smaller than those due to the other terms appearing in the Hamiltonian (11) and its contribution can be neglected for the determination of the energy levels below 1 eV. The cubic CF Hamiltonian is given by [27]

$$H_{\text{CF}} = \tilde{B}_{40}[C_0^4 + (\tfrac{5}{14})^{1/2}C_4^4] + \tilde{B}_{60}[C_0^6 - (\tfrac{7}{2})^{1/2}C_4^6] \tag{12}$$

where C_q^k are Racah tensor operators and $\tilde{B}_{kq}$ are the coefficients of the CF potential.

In the RS or intermediate coupling (IC) schemes, equation (12) may be substituted by [28]

$$H_{\text{CF}} = V_4\beta[\hat{O}_4^0(J) + 5\hat{O}_4^4(J)] + V_6\gamma[\hat{O}_6^0(J) - 21\hat{O}_6^4(J)] \tag{13}$$

where $\hat{O}_n^m(J)$ are Stevens operator equivalents, β and γ are reduced matrix elements for the J manifold and $V_n = A_n\langle r^n\rangle$, where $\langle r^n\rangle$ are the expectation values of the r^n operator over the 5f wavefunction. Equation (13) can also be written in terms of the parameters x and W of Lea *et al* [29] as

$$H_{\text{CF}} = W\left[\frac{x}{F(4)}(\hat{O}_4^0 + 5\hat{O}_4^4) + \frac{1-|x|}{F(6)}(\hat{O}_6^0 - 21\hat{O}_6^4)\right] \tag{14}$$

where $F(4)$ and $F(6)$ are numerical factors depending on J only and W is a common scaling factor for V_4 and V_6.

The following relations hold between the parameters appearing in equations (12)–(14):

$$\tilde{B}_{40} = 8\frac{xW}{\beta F(4)} = 8V_4 \tag{15a}$$

$$\tilde{B}_{60} = 16\frac{1-|x|}{\gamma F(6)}W = 16V_6. \tag{15b}$$

The diagonalization of the Hamiltonian (10) has been carried out by taking into account J-mixing by the CF using the program SHELL [30] and the parameters of the free ion Hamiltonian H_{int} reported in [31]. As a first step, H_{ion} has been diagonalized

Table 1. The lowest eleven eigenvalues of the free ion Hamiltonian of Np^{4+}. The Slater integral parameters $F^{(2)} = 5713.5$ meV, $F^{(4)} = 5206.5$ meV, $F^{(6)} = 3359.4$ meV and the spin–orbit parameter $\zeta_{SO} = 259.7$ meV have been used.

$\|\alpha, J\rangle$	E (meV)
$\|1,9/2\rangle$	0
$\|1,11/2\rangle$	675.7
$\|1,3/2\rangle$	948.3
$\|1,13/2\rangle$	1256.2
$\|1,5/2\rangle$	1399.3
$\|2,9/2\rangle$	1438.3
$\|2,5/2\rangle$	1593.9
$\|2,3/2\rangle$	1614.9
$\|1,7/2\rangle$	1697.1
$\|1,15/2\rangle$	1762.3
$\|2,7/2\rangle$	1925.1

on the RS basis and the IC states $|\alpha JM\rangle$ have been built up. The Slater integrals and the spin–orbit parameter used are given in table 1 together with the eigenvalues of the first eleven low-lying $|\alpha JM\rangle$ levels which were used as a truncated basis for the diagonalization of the complete Hamiltonian. This last step was performed for different values of the ratio V_6/V_4 as a function of V_4. For all the considered values of the CF parameters the ground state was the $\Gamma_8^{(2)}$ quartet. The resulting energy separation between the ground state and excited $\Gamma_8^{(1)}$ and Γ_6 levels is shown in figure 7.

Since only one magnetic transition has been observed, an unambiguous determination of H_{CF} from the spectroscopy results alone is, clearly, not possible. However, complementary information come from the study of the isostructural compound UO_2, for which the complete CF spectrum is known from neutron spectroscopy. The data obtained for UO_2 suggest two possible values for the ratio of sixth- to fourth-order CF potentials in NpO_2. In fact, V_4 and V_6 may be estimated from the values determined for UO_2, namely $V_4^U = -123$ meV and $V_6^U = 26.5$ meV [2, 3]. Using the relativistic determination of the radial integrals for Np^{4+} [21], $\langle r^4\rangle = 6.5$ au and $\langle r^6\rangle = 37.8$ au, and neglecting the small difference in the metal–ligand distances in the two cases, one obtains for Np: $V_4 = -105$ meV, $V_6 = 21$ meV and $V_6/V_4 = -0.2$ ($x = -0.48$, $W = -3.8$ meV). Figure 7 shows that these parameters lead to a $\Gamma_8^{(2)}$–$\Gamma_8^{(1)}$ splitting in line with the position of the observed CF transition. We remark that in terms of the Newman superposition model [32] they give intrinsic single-ligand CF parameters $\bar{A}_4 = 34$ meV and $\bar{A}_6 = 12$ meV, in satisfactory agreement with the results of superposition model analysis in other systems [33].

A second possibility for the V_6/V_4 ratio, corresponding to a smaller J-mixing effect, has been considered in order to allow a better comparison with previous theoretical approaches [8]. This may be obtained by scaling to the NpO_2 case the RS parameters which give a good fit to the UO_2 splittings. By taking $W^U = 4.3$ meV and $x^U = 0.9$ [3], we obtain, for Np, $W = -1.74$ meV and $x = -0.75$, that is $V_4 = -75$ meV, $V_6 = 4.5$ meV and $V_6/V_4 = -0.06$. This leads to a splitting of about 50 meV between the two Γ_8 quartets in the RS approximation.

As will be discussed later, the physical characteristics of the system are mainly determined by the value of the V_6/V_4 ratio. Then, it seems reasonable to assume

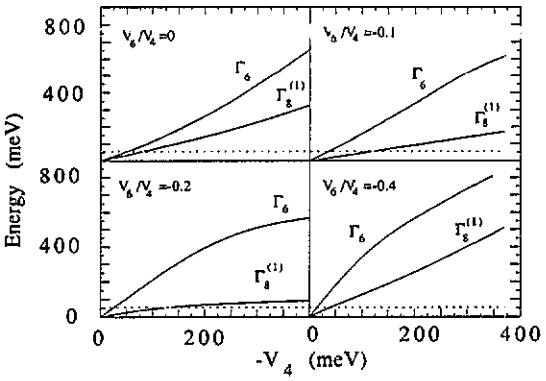

Figure 7. Energy differences between the ground and the excited states calculated as a function of the fourth-order potential V_4 and the ratio V_6/V_4. The broken curves are drawn at 55 meV.

as CF parameters for NpO_2 those obtained by keeping V_6/V_4 fixed at each of the values obtained earlier, and, by varying V_4 in order to fit the experimental value of about 55 meV observed for the centroid of the inelastic peak in the neutron scattering spectra. Using this criterion and the J-mixing results of figure 7, the set of parameters $V_4 = -104$ meV and $V_6 = 6.2$ meV ($x = -0.75$, $W = -2.4$ meV) is obtained for $V_6/V_4 = -0.06$, while $V_4 = -132$ meV and $V_6 = 26.4$ meV ($x = -0.48$, $W = -4.8$ meV) is found if the ratio $V_6/V_4 = -0.2$ is assumed. The first case, that we will call case a, is a weak-CF solution with a negligible J-mixing effect, while J-mixing effects are considerably more important if the second set of parameters (case b) is adopted. In case a, the Γ_6 is predicted at 145 meV while in case b, the position of the Γ_6 doublet would be at 274 meV.

In order to discuss the interpretation of neutron scattering data, the transition probabilities from the ground to the excited states must be calculated. We use an expression for the transition probability matrix elements in the magnetic dipole approximation between the multiplets Γ_n and Γ_m (see equation (1)) generalized for the case of J-mixing calculations. For a powder sample we have

$$P(\Gamma_n \rightarrow \Gamma_m) = \tfrac{1}{3}\sum_{\alpha}\sum_{\mu,\nu}|\langle\Gamma_n^{\nu}|L_\alpha + 2S_\alpha|\Gamma_m^{\mu}\rangle|^2 \tag{16}$$

with $\alpha = x, y, z$. Figure 8 shows the results obtained as a function of V_4 for different values of the V_6/V_4 ratio. It can be seen that $P(\Gamma_8^{(2)} \rightarrow \Gamma_6)$ is considerably smaller than $P(\Gamma_8^{(2)} \rightarrow \Gamma_8^{(1)})$, at least in the range of parameters which is physically interesting. In case a, the intensity of the $\Gamma_8^{(2)} \rightarrow \Gamma_6$ excitation is almost zero. In case b it is at least four times weaker than the $\Gamma_8^{(2)} \rightarrow \Gamma_8^{(1)}$ transition. In both cases we therefore expect to be able to observe just one CF peak corresponding to the $\Gamma_8^{(2)} \rightarrow \Gamma_8^{(1)}$ excitation. However, two sub-peaks separated by about 25 meV are revealed by the experiment. This splitting is unlikely to be attributed to the presence of hydrogen contamination, as was found in a recent neutron scattering study on Pu dioxide [34]. The energy of the observed transition is in fact too low, and in a range where no inelastic scattering was observed from PuO_2. Moreover, the observed Q dependence of the intensity is not a characteristic of hydrogen vibrational modes [35].

We shall return to the nature of the two peaks after considering the ordered phase.

5.2. The ordered phase

Several theoretical models have attempted to explain the phase transition observed in NpO_2 below $T_c = 25$ K. As already mentioned, Friedt *et al* [9] proposed a dynamic internal distortion of the oxygen sublattice below $T_c = 25$ K. The resulting reduction in the local symmetry induces a splitting of the cubic CF multiplets such as to reduce the magnetic susceptibility $\chi(T)$ as the temperature falls below T_c. This hypothesis is consistent with the Mössbauer results but in contradiction with a search for anharmonic effects at low temperature by neutron diffraction [10]. Zolnierek *et al* [36] have advanced the hypothesis that in NpO_2 the cation is trivalent. This model is, however, in contradiction with both the isomer shift in Mössbauer spectra and the magnetic form factor measured by neutron diffraction [20] which establishes a tetravalent $5f^3$ electronic configuration.

In analogy to the UO_2 case, Solt and Erdös [37] assume a collective Jahn–Teller monoclinic distortion of the oxygen sublattice driven by the quadrupolar interaction. As a consequence of this distortion, the Np^{4+} quadrupoles order in an antiferroquadrupolar configuration and the $\Gamma_8^{(2)}$ quartet is split into two Kramers doublets, the lowest one being nearly non-magnetic provided that the relative strength of the fourth and sixth-order cubic CF assumes a particular value and that the anisotropy confines the magnetic moment to the [001] direction. The previous neutron diffraction experiments have looked for this static distortion without success but the appearance of a magnetic excitation below $T_c = 25$ K, indicating a splitting of the $\Gamma_8^{(2)}$ quartet, is indirect evidence that an internal distortion of the oxygen–ligand cage does indeed take place. We have no experimental information on the symmetry of the actual distortion, which could be different from the one observed in UO_2 and assumed in the theoretical analysis given in [37]. In fact, the neutron diffraction results obtained for the $U_{1-x}Np_xO_2$ solid solutions [25, 26] revealed a magnetic order in the Np-rich compounds which is different from the one exhibited by UO_2. Therefore, the situation in the pure NpO_2 could be different even from the one present in the (U,Np) solid solutions.

In absence of experimental information on the detailed geometry of the lattice distortion, we have chosen to analyse the data in the case of the monoclinic distortion assumed in [37], corresponding to the condensation of the M_5 optic phonon mode. The point symmetry at the Np site is, in that case, lowered to C_{2h}. In a reference frame with the z-axis parallel to the [001] crystallographic direction and the x-axis along the [110] direction, pointing towards the pair of oxygen ions which become closer under distortion, the CF Hamiltonian is given by

$$H_{CF} = H_{cub} + H_{dist} \tag{17}$$

where H_{cub} is obtained from equation (12) by changing the sign of the off-diagonal components (because of the axial rotation of the reference frame), and

$$H_{dist} = \tilde{B}_{22}C_2^2 + \tilde{B}_{42}C_2^4 + \tilde{B}_{62}C_2^6 + \tilde{B}_{66}C_6^6. \tag{18}$$

The relations between the $\tilde{B}_{kq}$ and the coefficients usually appearing in the RS or IC approximation are given in table 2. It should be noted that the omission of the

Table 2. Relations between the coefficient $\tilde{B}_{kq}$ of the J-mixing CF Hamiltonian and the parameters A_{kq} usually appearing in the RS or IC approximations; $\langle r^k \rangle$ are the expectation values of the r^k operators over the 5f wavefunction.

$\tilde{B}_{20} = A_{20}\langle r^2 \rangle$	$\tilde{B}_{22} = (2/3)^{1/2}\ A_{22}\langle r^2 \rangle$
$\tilde{B}_{42} = 4 \times 10^{-1/2}\ A_{42}\langle r^4 \rangle$	$\tilde{B}_{43} = -2 \times 35^{-1/2} \times A_{43}\langle r^4 \rangle$
$\tilde{B}_{44} = 8 \times 70^{-1/2}\ A_{44}\langle r^4 \rangle$	$\tilde{B}_{63} = -8 \times 105^{-1/2}\ A_{63}\langle r^6 \rangle$
$\tilde{B}_{62} = 16 \times 105^{-1/2}\ A_{62}\langle r^6 \rangle$	$\tilde{B}_{66} = 16 \times 231^{-1/2}\ A_{66}\langle r^6 \rangle$
$\tilde{B}_{64} = (16/3) \times 14^{-1/2}\ A_{64}\langle r^6 \rangle$	

other symmetry-allowed terms in equation (18) causes an error in the energy level positions which is negligible for the small distortions considered here [3].

It can be shown that the term H_{dist} is equivalent to the quadrupolar Hamiltonian used in [37] to describe the perturbation induced by the distortion.

The parameters appearing in equation (18) have been calculated in the nearest-neighbour point-charge (PC) approximation for different oxygen fractional displacement $\delta = \Delta/a$.

The diagonalization of the total Hamiltonian (10), with H_{CF} given by equation (17), has been performed using the PC values for the distortion term and by varying $\tilde{B}_{40}$ for fixed $\tilde{B}_{60}/\tilde{B}_{40}$ ratios (i.e. by varying V_4 for fixed V_6/V_4). As a result of the distortion, each quartet is split into two Kramers doublets while the energy of the Γ_6 doublet remains essentially unperturbed. The calculated splitting is about 6 meV for $\delta = 0.004$ ($\Delta = 0.022$ Å) when we assume for the cubic part the CF parameters corresponding to case a. In contrast, a similar splitting can be obtained in case b only for $\delta \approx 0.006$ ($\Delta = 0.033$ Å), which is slightly higher than the upper limit given in [12]. These results would suggest that the values $V_4 = -104$ meV and $V_6 = 6.2$ meV of case a should be used for the cubic part of the CF Hamiltonian. However, the parameters of case b cannot be unambiguously rejected because, as discussed in [3], the PC parameters used for the distortion term (18) could be underestimated, due to the limits intrinsic to the PC approximation.

Table 3. Transition probabilities between the ground state Ψ_1 and the levels Ψ_i in NpO_2 ($i = 1$–5) calculated in J-mixing approximation under an internal distortion with amplitude $\delta = 0.004$. Two sets of parameters are used for the cubic CF Hamiltonian: (*a*) $V_4 = -104$ meV and $V_6 = 6.2$ meV; (*b*) $V_4 = -132$ meV and $V_6 = 26.4$ meV.

	$P(\Psi_1 \rightarrow \Psi_1)$	$P(\Psi_1 \rightarrow \Psi_2)$	$P(\Psi_1 \rightarrow \Psi_3)$	$P(\Psi_1 \rightarrow \Psi_4)$	$P(\Psi_1 \rightarrow \Psi_5)$
(*a*)	3.79	1.74	1.42	2.04	0.01
(*b*)	1.37	2.08	2.54	1.18	0.80

The probabilities of transition between the ground doublet Ψ_1 and the doublets Ψ_i ($i = 1$–5) are given in table 3 for both cases a and b and for $\delta = 0.004$. Also in case b the intensity of the transition to the Γ_6 level is still too small to be observed, since absorption resonances and the reduction of the form factor make the experiment difficult in the energy region above 200 meV.

In [37] Solt and Erdös found that for the assumed monoclinic distortion, the z-component of the magnetic moment of the lowest doublet vanishes for a ratio between the V_6 and V_4 parameters very close to -0.06. In this case, the system has a zero ordered moment if an anisotropy mechanism forces the magnetic moment

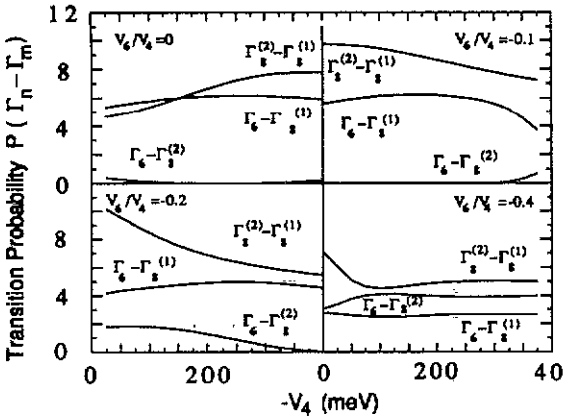

Figure 8. Transition probability matrix elements $P(\Gamma_n \rightarrow \Gamma_m)$ between the cubic CF multiplets of NpO_2 calculated in J-mixing approximation as a function of V_4 and the ratio V_6/V_4.

along the [001] axis. It can be seen that the magnetic moment components essentially depend, as stated before, on the value of V_6/V_4 while they are little influenced by variations of the V_4 parameter. In order to facilitate the comparison with the RS results in [37] we show in figure 9 the μ_i $(i = x, y, z)$ obtained, as a function of the Lea–Leask–Wolf (LLW) [29] x parameter, for $W = -2.4$ meV and $W = -4.8$ meV. Figure 9 shows that in the RS approximation $\mu_z = 0$ for $x = -0.73$, while J-mixing calculations give $\mu_z = 0$ for $x = -0.75$ (if $W = -2.4$ meV) or $x = -0.85$ (if $W = -4.8$ meV). Therefore, in case a, μ_z is almost zero and this could explain the lack of magnetic order below T_c if an anisotropy mechanism exists that forces the magnetic moment to lie along the z direction. Under these conditions, μ_x and μ_y would also be zero and the constant value observed for the magnetic susceptibility χ below 5 K would be explained. On the other hand, if the moment is free, $\chi(T)$ should diverge as T goes to zero even if $\mu_z = 0$.

6. The magnetic susceptibility and entropy

As regards the magnetic susceptibility, we have to distinguish between the two regions below and above T_c. In the first region, we notice that the single-ion interactions considered in the framework of the present CF analysis cannot account for the constant behaviour of the susceptibility at low temperature. In fact, the ground state wavefunction is strongly anisotropic and we can obtain a vanishingly small magnetic moment only by forcing it to lie in a given direction through a mechanism which is likely to be related to interionic effects. On the other hand, as discussed in [9], a weakly anisotropic ground doublet, with low values of the magnetic moment components, could be obtained with a lattice distortion which has a different symmetry from the one considered here. However, in that case the susceptibility starts to diverge well above 5 K, unless an unphysically large oxygen displacement is assumed [10]. In the paramagnetic region, from 77 to 280 K, the inverse susceptibility follows a modified Curie–Weiss law (MCW). The renormalized effective moment [38] is $\mu_{\text{eff}} \approx 2.7\ \mu_B$, which is somewhat smaller than that expected for the two proposed sets of CF parameters. This can be seen in figure 10, which shows the comparison between the Van Vleck susceptibility, calculated in absence of exchange effects, and the experimental curve. In both cases a and b, the slope of the theoretical χ^{-1} curve is smaller

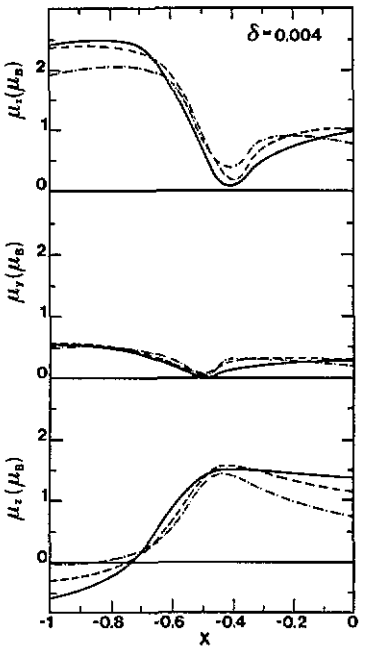

Figure 9. Components of the Np magnetic moment in the ordered phase of NpO_2 as a function of the Lea *et al* parameter x. A monoclinic distortion with amplitude $\delta = 0.004$ is assumed: full curve, RS approximation; broken curve, J-mixing calculations with $W = -2.4$ meV; and chain line, J-mixing calculations with $W = -4.8$ meV. The two sets of cubic CF parameters discussed in the text corresponds to (*a*) $x = -0.75$, $W = -2.4$ meV and (*b*) $x = -0.48$, $W = -4.8$ meV.

than the measured one. To achieve a value of μ_{eff} close to the experimental one, in this temperature range, the value of V_4 should be increased by at least a factor two. However, with $V_4 \sim 250$ meV the splitting between the two Γ_8 quartets would increase to ~ 145 meV in case a and to ~ 75 meV in case b, while no magnetic excitations are seen in the neutron spectra at those energies. This apparent disagreement between CF spectroscopy and magnetic susceptibility results has been observed in all the actinide dioxides studied so far with both techniques, namely UO_2, NpO_2 and PuO_2. This is probably due to the fact that, as in the paramagnetic phase, a single-ion picture, even allowing for exchange effects in a molecular-field approach, is inadequate to account for the behaviour of these compounds. Above the transition temperature, the magnetic susceptibility could be affected by short-range order and magnetic fluctuations, as well as by magnetoelastic interactions, which in UO_2 are known, from the behaviour of the elastic constant [39], to be effective up to room temperature. The situation is different in magnetically diluted $An_xTh_{1-x}O_2$ (An ≡ U, Pu) solid solutions, where better consistency between neutron spectroscopy results and magnetic susceptibility is achieved [40, 41].

To support the proposed CF scheme, we look at the magnetic entropy S_m above 100 K, that is sufficiently far from the transition point to be sure that the f-electron contribution to S_m is mainly due to the population of the CF levels. In figure 11 the experimental values given in [7] up to ~ 300 K are compared with the theoretical curve. Essentially the same result is obtained with both sets a and b of CF parameters, because they correspond to the same energy separation between the $\Gamma_8^{(2)}$ and the $\Gamma_8^{(1)}$ quartets, while the Γ_6 doublet is too high in energy to contribute significantly to S_m in this temperature range. The agreement with the experiment is quite good taking into account the approximations involved. It must be noticed that a 10% reduction in the splitting between the two quartets is sufficient to give the best fit to the experimental data.

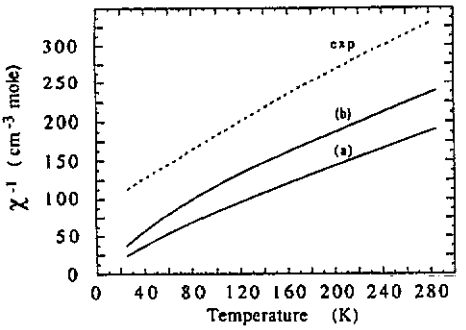

Figure 10. Comparison between the calculated inverse Van Vleck magnetic susceptibility and the experimental curve (broken curve). The full curves correspond to the CF parameters of cases a and b discussed in the text.

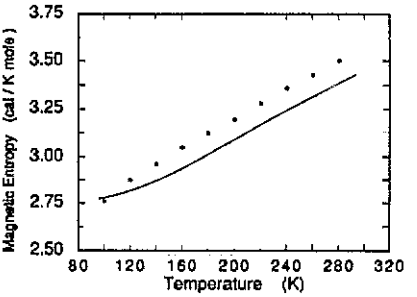

Figure 11. Comparison between the experimental magnetic entropy (•) and the curve calculated using the CF parameters of both cases a and b (full curve).

7. Discussion and conclusions

In this paper we have analysed the CF neutron spectroscopy results for NpO_2. The situation in this compound is clearly quite different from that of UO_2. In the latter system extremely sharp well defined CF states have been seen [3], and a relatively complete assignment of the parameters can be made. This is not the case in NpO_2. Whereas the splitting of the ground state $\Gamma_8^{(2)}$ below 25 K is relatively sharp (see figure 6) the principal CF splitting $\Gamma_8^{(2)} \rightarrow \Gamma_8^{(1)}$ results in a wide band with intensity in the region 30 to 100 meV (see figure 4). This is exactly the energy range anticipated for the transition based on a relatively constant A_4 and A_6 across the actinide dioxide series, but there is not immediate explanation for its broad nature. The second transition $\Gamma_8^{(2)} \rightarrow \Gamma_6$ has too small a matrix element to be visible (see figure 8), although we have searched up to energy transfers of 350 meV using incident energies up to 1100 meV.

The broadening of the $\Gamma_8^{(2)} \rightarrow \Gamma_8^{(1)}$ transition may be caused by a number of mechanisms. However, it is important to note that only in NpO_2 in the actinide dioxides does the strongest CF transition lie below the phonon cut-off of 80 meV. In addition, a strong phonon exists at ~ 55 meV (see figure 1) and is known to be of Γ_{25}' symmetry from the work of Dolling *et al* on UO_2 [42]. The Γ_8 modes can couple strongly to this mode as has been discussed in $CeAl_2$ [43,44]. It seems possible, therefore, that the splitting of the $\Gamma_8^{(2)} \rightarrow \Gamma_8^{(1)}$ mode is due to an interaction between electronic and vibronic parts of the spectra. In the absence of such an interaction the excitation energy would be ~ 55 meV. Further progress in understanding this would require neutron experiments on single crystals, which are not presently available of sufficient size for such investigations.

Taking into account the results from UO_2 we have proposed two possible CF models, which differ only in their details. The most important finding of our study is the unambiguous proof by using neutron polarization analysis that the ground state $\Gamma_8^{(2)}$ splits at 25 K into (almost certainly) two doublets. This is the first microscopic evidence shed on this intriguing transition, first discovered by bulk measurements in

1953 [7]. Our observations strongly suggest that a crystallographic phase transition occurs due to the ordering of the quadrupoles in NpO_2, in a similar fashion to that found in UO_2.

The upper limits set by diffraction experiments for the oxygen displacement are quite stringent but we have shown that the observed energy splitting may be accounted for by distortion amplitudes close to these limits. The calculations were made by assuming an internal monoclinic distortion as proposed for NpO_2 by Solt and Erdös [37] to explain the nearly zero value of the ordered moment. Although both CF solutions suggested above are in line with the experimental result, in the case of the smaller V_6/V_4 ratio the CF is more effective in splitting the $\Gamma_8^{(2)}$ quartet and leads to an almost zero value of μ_z. However, the second solution also gives rise to a strong reduction in the ordered moment component along the [110] direction. This case is rather interesting because it seems to describe very nicely what has been observed by neutron diffraction and Mössbauer spectroscopy in the $U_{1-x}Np_xO_2$ solid solution [26] with $x \leqslant 0.25$. In fact, these compounds order antiferromagnetically with the same magnetic structure as UO_2. It is likely that below T_N the oxygen sublattice undergoes a distortion similar to the one described above. The effective exchange field due to the U^{4+} ions could then force the Np moments to lie along the [110] direction. In this case, the ordered moment on the Np site would be given by the value of the μ_x component which is very close to the measured one, $\mu_0 \sim 0.5\ \mu_B$.

Therefore, we are left with the two following possibilities:

(i) the concentrated compound and the diluted solid solution ($x < 0.5$) have a similar behaviour and the zero value of the ordered moment in NpO_2 is due to effects not considered in the present approach;

(ii) the concentrated compound has a peculiar situation in which the interionic interactions tend to orient the moment along the [001] direction and the CF is such to produce a zero value of the moment as originally proposed by Solt and Erdös [37].

Case (i) corresponds to the proposed solution b, while case (ii) is in line with solution a for the CF parameters.

We conclude that the results here presented allows us to go further in the understanding of the mysterious NpO_2 problem and to restrict the field of the possible explanations, although we cannot choose at present between the two possibilities outlined earlier in the framework of the considered CF model.

Acknowledgments

We wish to thank J Larroque at Cadarache for preparing the sample used at RAL and J Rebizant at Karlsruhe for encapsulating the sample used at ILL. All safety considerations for these experiments were handled with considerable skill by the ISIS and ILL Radioprotection Services, to whom we owe our thanks. This work was supported in part by Istituto Nazionale di Fisica della Materia e dal Gruppo Nazionale di Struttura della Materia (Consiglio Nazionale delle Ricerche), Italy and in part by the underlying research programme of the UK Atomic Energy Authority.

References

[1] Kern S, Loong C K and Lander G H 1985 *Phys. Rev.* B **32** 3051

[2] Osborn R, Taylor A D, Bowden Z A, Hackett M A, Hayes W, Hutchings M T, Amoretti G, Caciuffo R, Blaise A and Fournier J M 1988 *J. Phys. C: Solid State Phys.* **21** L931
[3] Amoretti G, Blaise A, Caciuffo R, Fournier J M, Hutchings M T, Osborn R and Taylor A D 1989 *Phys. Rev.* B **40** 1856
[4] Amoretti G, Blaise A, Fournier J M, Caciuffo R, Larroque J, Osborn R, Taylor A D and Bowden Z A 1988 *J. Magn. Magn. Mater.* **76–7** 432
[5] Amoretti G, Blaise A, Caciuffo R, Fournier J M, Larroque J and Osborn R 1989 *J. Phys.: Condens. Matter* **1** 5711
[6] Dunlap B D and Kalvius G M 1985 *Handbook on the Physics and Chemistry of the Actinides* vol 2, ed A J Freeman and G H Lander (Amsterdam: Elsevier) p 329
[7] Osborne D W and Westrum Jr E F 1953 *J. Chem. Phys.* **21** 1884
[8] Erdös P, Solt G, Zolnierek Z, Blaise A and Fournier J M 1980 *Physica* B **102** 164
[9] Friedt J M, Litterst F J and Rebizant J 1985 *Phys. Rev.* B **32** 257 and references therein
[10] Caciuffo R, Lander G H, Spirlet J C, Fournier J M and Kuhs W F 1987 *Solid State Commun.* **64** 149 and references therein
[11] Boeuf A, Caciuffo R, Fournier J M, Manes L, Rebizant J, Spirlet J C and Wright A 1983 *Phys. Status Solidi* **79** K1
[12] Boeuf A, Fournier J M, Heger G, Manes L, Rebizant J, Rustichelli F and Spirlet J C 1981 *J. Physique Lett.* **42** L-401
[13] Faber Jr J and Lander G H 1976 *Phys. Rev.* B **14** 1151
[14] Lander G H, Faber Jr J, Freeman A J and Desclaux J P 1976 *Phys. Rev.* B **13** 1177
[15] Erdös P and Robinson J M 1983 *The Physics of Actinides Compounds* (New York: Plenum) p 142
[16] Kern S, Morris J, Loong C-K, Goodman G, Lander G H and Cort B 1988 *J. Appl. Phys.* **63** 3598
[17] Fournier J M, Blaise A, Amoretti G, Caciuffo R, Larroque J, Hutchings M T, Osborn R and Taylor A D 1991 *Phys. Rev.* B **43** 1142
[18] Caciuffo R, Amoretti G, Fournier J M, Blaise A, Osborn R, Taylor A D and Hutchings M T 1991 *Solid State Commun.* **79** 197
[19] Stirling W G and McEwen K A 1987 *Methods of Experimental Physics* vol 23 part C, ed K Sköld and D L Price (Orlando: Academic)
[20] Delapalme A, Forte M, Fournier J M, Rebizant J, Spirlet J C 1980 *Physica* B **102** 171
[21] Desclaux J P and Freeman A J 1978 *J. Magn. Magn. Mater.* **8** 119
[22] Moon R M, Riste T and Koehler W C 1969 *Phys. Rev.* **181** 920
[23] Taylor A D, Boland B C, Bowden Z A and Jones T J L 1987 *Rutherford Appleton Laboratory Report No RAL-87-012*
[24] Osborn R 1991 unpublished
[25] Tabuteau A, Pages M, Boeuf A, Rebizant J, Manes L, Caciuffo R and Rustichelli F 1984 *J. Physique Lett.* **45** L373
[26] Boeuf A, Caciuffo R, Pagès M, Rebizant J, Rustichelli F and Tabuteau A 1987 *Europhys. Lett.* **3** 221
[27] Wybourne B G 1965 *Spectroscopic Properties of Rare Earths* (New York: Wiley)
[28] Hutchings M T 1964 *Solid State Physics* vol 16, ed F Seitz and D Turnbull (New York: Academic) p 227
[29] Lea K R, Leask M J M and Wolf W P 1962 *J. Phys. Chem. Solids* **23** 1381
[30] Crosswhite H N and Crosswhite H 1984 *J. Opt. Soc. Am.* B **1** 246
[31] Carnall W T and Crosswhite H N 1985 *Argonne National Laboratory Report ANL-84-90*
[32] Newman D J and Ng B 1989 *Rep. Prog. Phys.* **52** 699
[33] Newman D J and Ng B 1989 *J. Phys.: Condens. Matter* **1** 1613
[34] Kern S, Loong C-K, Goodman G L, Cort B and Lander G H 1990 *J. Phys.: Condens. Matter* **2** 1933
[35] Stirling W G, McEwen K A and Loong C-K 1986 *Physica* B **136** 420
[36] Zolnierek A, Solt G and Erdös P 1981 *J. Phys. Chem. Solids* **42** 773
[37] Solt G and Erdös P 1980 *J. Magn. Magn. Mater.* **15–18** 57
[38] Amoretti G and Fournier J M 1984 *J. Magn. Magn. Mater.* **43** L217
[39] Brandt O G and Walker C T 1968 *Phys. Rev.* **170** 528
[40] Sasaki K and Obata Y 1971 *J. Phys. C: Solid State Phys.* **32** 1–739
[41] Candela G A, Hutchinson Jr C A and Lewis W B 1959 *J. Phys. Chem.* **30** 246
[42] Dolling G, Cowley R A and Woods A D B 1965 *Can. J. Phys.* **43** 1397
[43] Thalmaier P and Fulde P 1982 *Phys. Rev. Lett.* **49** 1588
[44] Thalmaier P 1984 *J. Phys. C: Solid State Phys.* **17** 4153